Solving the time-dependent Schrödinger equation using complex-coordinate contours

C. William McCurdy, Carrie K. Stroud, and Matthew K. Wisinski
Department of Chemistry, The Ohio State University, 120 West Eighteenth Avenue, Columbus, Ohio 43210
(Received 25 July 1990; revised manuscript received 19 November 1990)

The complex-coordinates approach in scattering theory is extended to the time-dependent Schrödinger equation by using Simon's exterior scaling contour, and it is shown to cause outgoing wave packets to vanish for large distances in collision problems. Numerical applications are given for one- and two-dimensional problems where the complex-coordinates method is shown to eliminate reflections of outgoing wave packets from the boundaries of the coordinate space grid used in the calculations. The extension of the exterior scaling approach to the time-dependent description of a charged particle in dc and ac electromagnetic fields is given, and numerical results on these problems are also presented.

I. INTRODUCTION

The use of complex-coordinate techniques in calculations on scattering resonances and for the calculation of scattering and photoionization amplitudes has been commonplace since the early 1970's. The consequences of simply scaling the coordinates x in the Hamiltonian by a complex factor according to $x \rightarrow xe^{i\theta}$, as well as more complicated analytic continuations, have been exploited in numerous applications of the idea. The numerical applications have dealt, until very recently,[1,2] only with the time-independent formulation of collision theory or with time-periodic problems where the time dependence can be eliminated using Floquet theory.[3] We seek here to point out that the direct application of these ideas to solving the time-dependent Schrödinger equation (including the case of generally time-dependent Hamiltonians) leads to some interesting computational advantages, and, more importantly, completes an elegant picture of analytic continuation in quantum scattering theory that is only partially apparent in the time-independent formulation.

The application of complex-coordinate methods in many-body Coulomb systems is based on theorems due to Aguilar, Balslev, Combes, and Simon[4] on the spectrum of the analytically continued Hamiltonian $H(xe^{i\theta})$ for these systems. In particular, discrete resonance states are uncovered by this continuation and the associated wave functions become square integrable. Most of the early applications to resonances were in the electron-atom scattering problem,[5-9] but adaptations of the idea for electron-molecule collisions are by now also familiar.[10-12] The use of these ideas to compute Green's-function matrix elements, and therefore scattering and photoionization amplitudes is also well established,[13-18] and most of the formal and practical limitations of the approach are well understood.[19] The formal mathematical problems,[20,21] and some practical results,[3,22,23] for atoms in electromagnetic fields have been discussed, where the time dependence of the fields was treated by Floquet theory. There have also been several reviews[24-28] of the subject.

In this work we establish the extension of these ideas to the time-dependent Schrödinger equation and demonstrate their utility in problems which have intrinsic time dependence. In Sec. II, we show that correct choices of complex-coordinate continuations can cause outgoing wave packets leaving a collision to be extinguished exponentially beyond a designated point, while other choices cause outgoing packets to diverge and modify the large-distance behavior of incoming packets. The key to practical applications of complex coordinates to time-dependent problems is an analytic continuation of the coordinates, introduced by Simon[29] as a formal mathematical device, called "complex exterior scaling." In this approach the coordinates are continued onto a contour which is complex only beyond a certain distance. Exterior scaling can prevent reflection of wave packets from the boundaries of a finite grid used to represent their propagation, while leaving them unchanged in the regions of interest. This result has obvious practical consequences in numerical computations. The analytically continued packets do not reflect at the boundaries because they are exponentially decaying along appropriate complex rays in the complex plane, while their motion at small distances is unchanged. Depending on the initial conditions, a collision problem is thereby effectively mapped onto a finite region of space, and continuum motion becomes a peculiar type of bound motion. Thus the behavior of collisional wave packets is simplified by simply looking at them along well-chosen complex-coordinate contours. We previously discussed some preliminary numerical results using this approach,[1,2] but the idea is more general than we had suspected.

It is interesting to note that the evolution of wave functions for any complex scaling of coordinates in the Hamiltonian is markedly different than that exhibited by solutions of the Schrödinger equation in complex *time*. It appears that no complex time analytic continuation can mimic complex coordinates in this respect, in part because the complex-coordinate transformation affects continuum states differently than it does bound states.

In Sec. II we explore the complex-coordinate behavior of wave packets in the case of time-independent potentials, but the extension to time-dependent potentials is

 ©1991 The American Physical Society

(mostly) straightforward. If the potential is time dependent but short range, we show here that using the exterior scaling contour produces the same type of behavior at large distances as in the time-independent case. For an atom in an ac electromagnetic field, the potential is not short range, but we show in Sec. IV that by working in the appropriate gauge (the radiation gauge) the same behavior of wave packets along the exterior scaling contour is achieved as in the short-range case.

The principal result of this paper is more than a mathematical device to prevent spurious reflections of wave packets in practical calculations. There are other, quite successful, ways to accomplish that end.[30] Instead, the connection between time-independent applications of complex coordinates and the time-dependent formulation is our primary focus, as well as the extension to time-dependent Hamiltonians and the time-dependent description of atoms in fields. The results we present here also suggest that it may be possible to analytically continue wave packets from a complex-coordinates calculation to regions beyond that covered by finite grid representation.

In Sec. II we briefly summarize the complex-coordinates idea and extend it to the time-dependent Schrödinger equation. Sec. III describes the finite-element procedure we use in the numerical examples. Section IV discusses some specific numerical results for one- and two-dimensional motions and also describes the extension of the idea to charged particles in dc and ac electromagnetic fields. Some conclusions and speculations are given in Sec. V.

II. COMPLEX COORDINATES IN QUANTUM HAMILTONIAN DYNAMICS

In this section we summarize the basics of the time-independent application of complex coordinates in collision theory and extend the idea to the time-dependent Schrödinger equation. We specialize the discussion to one-dimensional systems for notational simplicity. The generalization of the complex-coordinates approach to multidimensional time-independent systems is well known, and we shall present a multidimensional application to a time-dependent problem in Section IV D.

A. Complex coordinates in the time-independent Schrödinger equation

The idea of exploiting, both formally and in numerical calculations, the analytic continuation of spatial coordinates in the time-independent Schrödinger equation (TISE) is a venerable one, and there exists an extensive literature on the subject.[4–29] Here, we will describe only the essence of the idea without concerning ourselves with the well-known mathematical subtleties,[4,19] which require more rigor than we need to introduce the time-dependent generalization below.

The use of complex coordinates in the TISE is based on theorems[4] applicable to a wide class of Hamiltonians which are called "dilation analytic." The theorems describe the spectrum, shown in Fig. 1, of the Hamiltonian H_θ,

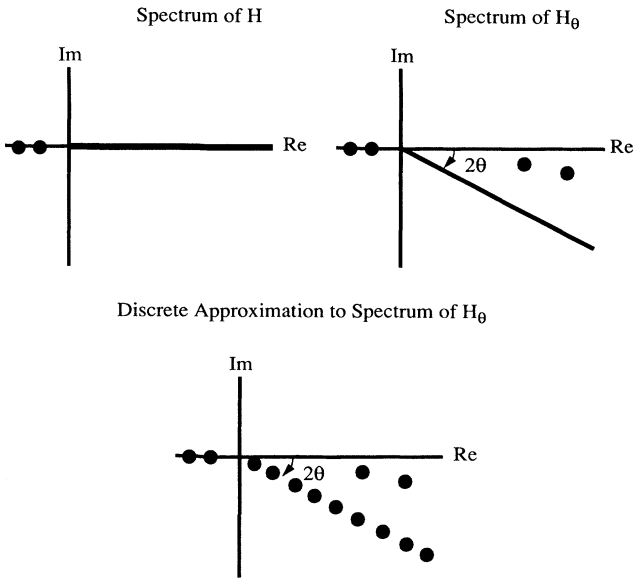

FIG. 1. Analytic continuation of the spectrum of a one-body Hamiltonian for the complex-coordinate continuation $xe^{i\theta}$ and for the contour $C(x)$.

$$H_\theta = H(xe^{i\theta}) , \tag{1}$$

in which the coordinates x have been scaled by $e^{i\theta}$. Subject to the boundary conditions that the eigenfunctions of $H(xe^{i\theta})$ be either zero or finite and oscillatory in the limit $x \to \infty$, the spectrum generally consists of discrete and continuous eigenvalues. The discrete eigenvalues appear at the bound-state energies of the original Hamiltonian $H(x)$ and at the complex resonance eigenvalues corresponding to poles of the S matrix. The continuous spectrum is rotated into the complex plane by an angle of -2θ.

The computational applications of this idea fall into two classes. The first is the computation of resonance eigenvalues, for which the eigenfunctions of $H(xe^{i\theta})$ are square integrable and thus can be computed by standard techniques for calculating bound-state eigenfunctions.[5–12] The second class of applications is the computation of Green's-function (resolvent) matrix elements[13,18] of the form $\lim_{\epsilon\to 0}\langle f|(E-H+i\epsilon)^{-1}|g\rangle$. An obvious way to try to compute this matrix element is to approximate the resolvent operator in terms of matrix eigenfunctions of the Hamiltonian. These eigenfunctions are approximations to the exact eigenfunctions ψ_E which satisfy

$$H\psi_E(x) = E\psi_E(x) , \tag{2}$$

and arise in any expansion of the exact eigenfunctions in a finite basis. The matrix eigenfunctions Φ_n and eigenfunctions E_n satisfy

$$\langle \Phi_n|H|\Phi_m\rangle = E_n\delta_{n,m} , \tag{3}$$

and the obvious approximate representation of a resol-

vent matrix element using N matrix eigenfunctions is

$$\lim_{\epsilon\to 0}\langle f|(E-H+i\epsilon)^{-1}|g\rangle \approx \sum_{n=1}^{N}\frac{\langle f|\Phi_n\rangle\langle\Phi_n|g\rangle}{(E-E_n)} . \quad (4)$$

This representation is useless for any N as it stands unless E lies outside the continuous spectrum of H, because it replaces the branch cut in the E plane, which lies along the continuous spectrum, with a row of discrete poles. Scattering amplitudes are expressed in terms of such matrix elements, and the scattering boundary conditions are contained in the $\epsilon\to 0$ limit. That information is discarded in Eq. (4).

However, if the functions $|f\rangle$ and $|g\rangle$ are appropriately bounded for large x then the integral implied in this matrix element is unchanged by the distortion of the integration contour onto the complex ray $xe^{i\theta}$. The resolvent matrix element now involves the analytically continued Hamiltonian H_θ. As has been discussed in depth in the complex-coordinates literature, the matrix eigenfunctions of H_θ are defined using an inner product without complex conjugation,

$$(\chi,\varphi)=\int_0^\infty \chi(x)\varphi(x)dx , \quad (5)$$

which we denote with parentheses. Denoting the matrix eigenfunctions and eigenvalues of H_θ by $\tilde{\Phi}_n$ and $\tilde{E}_n$, we see that they satisfy

$$(\tilde{\Phi}_n, H_\theta\tilde{\Phi}_m)=\tilde{E}_n\delta_{n,m} , \quad (6)$$

so that Eq. (4) becomes

$$\lim_{\epsilon\to 0}\langle f|(E-H+i\epsilon)^{-1}|g\rangle \approx \sum_{n=1}^{N}\frac{(f^*_{-\theta},\tilde{\Phi}_n)(\tilde{\Phi}_n,g_\theta)}{(E-\tilde{E}_n)} , \quad (7)$$

where $f_{-\theta}$ and g_θ denote $e^{-i(\theta/2)}f(xe^{-i\theta})$ and $e^{i(\theta/2)}g(xe^{i\theta})$ repsectively. The complex factors appearing in $f_{-\theta}$ and g_θ arise from the contour distortion in $\langle f|(E-H+i\epsilon)^{-1}|g\rangle$ that leads to Eq. (7). For a broad class of functions $|f\rangle$ and $|g\rangle$ this representation has been demonstrated[13–18] to be convergent with respect to increasing N, in sharp contrast to the representation in Eq. (4). This idea has been used, for example, in calculations of total photoionization cross sections of atoms and molecules.[14–17]

As a final note we observe that all of the results described in this section are unchanged if we replace analytic continuation of the coordinates onto the complex ray $xe^{i\theta}$ with continuation onto Simon's[29] "exterior scaling" contour defined by

$$C(x)=\begin{cases} x, & x<x_M \\ (x-x_M)e^{i\theta}+x_M, & x\geq x_M . \end{cases} \quad (8)$$

The exterior scaling contour, shown in Fig. 2(a), scales the coordinates only at large values of x and generalizes the complex-coordinates approach to a broader class of Hamiltonians containing potentials which are nonanalytic for $x<x_M$. Numerical application of this idea in resonance calculations is straightforward.[31] This contour also turns out to be useful in time-dependent applications of these ideas.

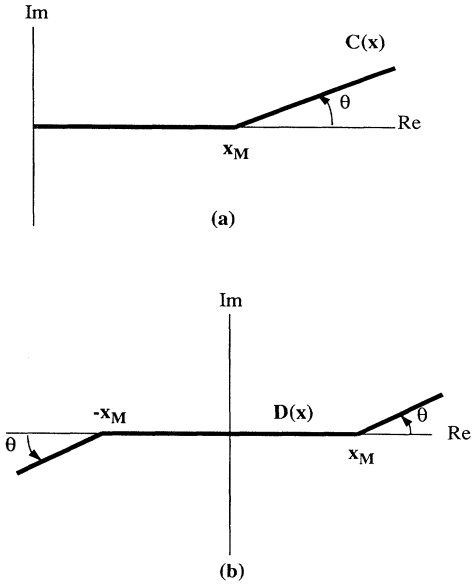

FIG. 2. Exterior complex scaling contours (a) for x on the interval $[0,\infty]$, (b) for x on the interval $[-\infty,\infty]$.

B. Complex coordinates in the time-dependent Schrödinger equation

In order to make the connection with the discussion of traditional applications of complex coordinates in the preceding section, we begin by considering a system for which the Hamiltonian is a function only of the coordinates x and not of time. This restriction will be lifted later in the discussion in Sec. IV where we present applications to the problem of a charged particle in an ac field.

In order to construct numerical solutions of the time-dependent Schrödinger equation (TDSE),

$$H\Psi(x,t)=i\hbar\frac{\partial}{\partial t}\Psi(x,t) , \quad (9)$$

we not only discretize time t in order to propagate the solution $\Psi(x,t)$, but we also discretize the coordinates in some way. This discretization may be carried out by using a grid of x values (in finite difference or Fourier-transform methods) or by using a set of square-integrable basis functions or finite elements. The effect is to place the x motion in some sort of "box," either in coordinate or Hilbert space, and to discretize the continuous spectrum of H as in Eq. (3). A familiar computational consequence of this discretization is that a wave packet describing unbounded motion will eventually reflect from the boundaries of the box and the results of the propagation will become unphysical.

While at first glance reflections from the boundaries of the coordinate or Hilbert space box appear to be a specific property of the time-dependent formulation, they are of course a manifestation of the numerical pathology

of Eq. (4). We can see that this is the case by using the matrix eigenfunctions of H, which are defined in Eq. (3) for any discretization of the x motion, to formally construct an approximation to the propagator

$$e^{-(i/\hbar)Ht} \approx U_N = \sum_{n=1}^{N} |\Phi_n\rangle e^{-(i/\hbar)E_n t} \langle \Phi_n| \ . \tag{10}$$

The resolvent matrix element we considered in the preceding section can be computed using the approximation in Eq. (10) to propagate $|g\rangle$ and Fourier-transforming the overlap of that packet with the function $|f\rangle$,

$$\lim_{\epsilon \to 0} \langle f|(E-H+i\epsilon)^{-1}|g\rangle$$

$$= -\frac{i}{\hbar} \lim_{\epsilon \to 0} \int_0^\infty e^{(i/\hbar)(E+i\epsilon)t} \langle f|e^{-(i/\hbar)Ht}|g\rangle dt \tag{11}$$

$$\approx -\frac{i}{\hbar} \lim_{\epsilon \to 0} \int_0^\infty e^{(i/\hbar)(E+i\epsilon)t} \langle f|U_N|g\rangle dt \tag{12}$$

$$= \sum_{n=1}^{N} \frac{\langle f|\Phi_n\rangle\langle\Phi_n|g\rangle}{(E-E_n)} \ . \tag{13}$$

The poles in Eq. (13) arise from the periodic behavior of the correlation function $\langle f|e^{-(i/\hbar)Ht}|g\rangle$ and in particular the poles in the continuum arise from periodic behavior due to the reflections from the edges of the "box" in which the motion is confined.

This elementary picture is not new of course, but it does suggest how the complex-coordinate approach can repair the long-time behavior of the correlation function and of the propagator in Eq. (10) (provided we are interested in sampling the propagated wave function in a finite region of space). The key is that using complex coordinates allows Eq. (7) to provide a convergent representation of the resolvent matrix element, and, as Eqs. (11)–(13) demonstrate, there is an equivalent approximation for the propagator in the form of Eq. (10).

The problem with translating the complex-coordinates approach, expressed in Eq. (7) for computing resolvent matrix elements, to a time-dependent representation is that we could thereby construct $\exp[-(i/\hbar)H_\theta t]$, which propagates wave packets for complex values of the coordinates. It would be of little appeal to construct $\Psi(xe^{i\theta},t)$ instead of $\Psi(x,t)$. However, if we pick a contour according to the exterior scaling procedure, we can construct solutions to the TDSE at real values of x in the region of interest.

For the moment consider a calculation which uses a discrete grid of x values, say using the finite-difference approach. If we pick a complex contour using the exterior scaling prescription in Eq. (8), we can keep the coordinates real for the region of interest while scaling only near the end of the grid. Using the contour $C(x)$ in Eq. (8) we would be constructing the propagator $\exp[-(i/\hbar)H(C(x))t]$. The important point is that, as Simon[29] showed, the Hamiltonian $H(C(x))$ has exactly the same spectrum as $H(xe^{i\theta})$, so that its discrete representation produces a well-behaved approximation in the form of Eq. (7) to resolvent matrix elements. That result is manifested in the fact that the time propagator $\exp[-(i/\hbar)H(C(x))t]$ based on $H(C(x))$ avoids the boundary reflection problem as long as a sufficiently accurate discrete representation is used. If the representation is sufficient to converge Eq. (7) for a range of energies, then there will be no spurious periodic motion arising from boundary reflections with frequencies corresponding to that energy range. In a previous publication[2] and in the following sections we present a finite-element implementation which demonstrates this fact for a variety of Hamiltonians, but we can see analytically how this procedure works by examining the propagation of a free packet on the contour $C(x)$.

We can write a free Gaussian wave packet, evaluated on the contour, in the form[32]

$$\Psi(C(x),t) = \exp\left[\frac{i}{\hbar}\alpha_t[C(x)-x_t]^2 + \frac{i}{\hbar}p_t[C(x)-x_t] + \frac{i}{\hbar}\gamma_t\right] , \tag{14}$$

where the position x_t and the other parameters are given by

$$x_t = x_0 + \frac{p_0}{m}(t-t_0) \ , \tag{15}$$

$$p_t = p_0 \ , \tag{16}$$

$$\alpha_t = \frac{\alpha_0}{\left[\frac{2}{m}\right]\alpha_0(t-t_0)+1} \ , \tag{17}$$

$$\gamma_t = -\frac{i\hbar}{4}\ln\left|\frac{2\alpha_0}{\pi\hbar}\right| + \frac{i\hbar}{2}\ln\left[\frac{2\alpha_0(t-t_0)}{m}+1\right] + \frac{p_0^2}{2m}(t-t_0) \ . \tag{18}$$

The momentum is constant for the free packet, and we take its value p_0 to be positive for the moment so that the packet propagates toward larger values of x. For simplicity we can also choose α_0 to be pure imaginary so the packet starts out as a real-valued Gaussian. Now as long as the value of θ in the contour $C(x)$, is less than $\pi/4$ the packet remains bounded,

$$\lim_{x \to \infty} \Psi(C(x)) = 0 \ , \tag{19}$$

but for $0 < \theta < \pi/4$ it goes to zero differently than does $\Psi(x,t)$ for large real values of x. In particular, the factor

$$\exp\left[\frac{i}{\hbar}p_t[C(x)-x_t]\right] = \exp\left[\frac{i}{\hbar}p_0[(x-x_M)e^{i\theta}+x_M-x_t]\right] \tag{20}$$

now goes to zero as x increases beyond x_M, while without analytic continuation $\exp[(i/\hbar)p_t(x-x_t)]$ continues to oscillate for large x. In particular, the factor in Eq. (20) goes to zero while other factors of the analytically contin-

ued packet continue to propagate outward, and thus the overall packet vanishes at all large x, *regardless of the time.* If the grid boundary is set far enough beyond x_M this outgoing packet will vanish before it reaches the boundary.

Thus an outgoing packet does *not* propagate forever if one looks at it on the contour $C(x)$. It begins to fall off exponentially as it propagates past x_M and cannot reflect from a boundary chosen sufficiently further out. In a suitably chosen discrete representation, this behavior eliminates the periodic oscillations in the box and is at the heart of the connection between the convergence of Eq. (7) and the ability of the corresponding discrete representation of $\exp[-(i/\hbar)H(C(x))t]$ to remain accurate for long times.

The contour, however, distorts the incoming packet if we start it beyond the point x_M. For the incoming packet we have $p_0<0$, so that the factor in Eq. (20) diverges for large x. Only the quadratic term in the exponent in Eq. (14) prevents the packet from diverging for large x and times greater than or equal to t_0. To use these ideas in practical scattering calculations we must choose the point x_M and the initial wave packet so that the incoming packet does not begin with appreciable amplitude beyond x_M.

Up to now we have treated x as though it were constrained to the interval $0<x<\infty$ but that is certainly not necessary. For the interval $-\infty<x<\infty$ we can choose a "double" exterior scaling contour $D(x)$ as shown in Fig. 2(b) and thereby eliminate reflections of packets which are outgoing to either positive or negative x.

It remains to establish the class of Hamiltonians for which complex contours can cause wave packets to vanish at large x instead of continuing to propagate outward. The arguments given in this section apply to any problem for which the potential $V(x)$ vanishes for large $|x|$ fast enough to allow the long time and large-x behavior of the wave packet to be expressed as some linear combination of outgoing Gaussian packets. A numerical application to such a problem in one dimension is given in the next section. If the Hamiltonian contains a time-dependent potential, but it is bounded in this way, our analysis of outgoing packets remains unchanged. Once the packet is beyond the range of the potential it can be expressed in terms of linear combinations of free Gaussian packets, and we have established their behavior on the contour $C(x)$.

The question of mathematically "long-range" potentials, such as the Coulomb potential, is more subtle. In Sec. IV D we give numerical results on a two-electron problem with Coulomb potentials, and we have reported one-dimensional Coulomb calculations previously.[2] The time-dependent complex contour approach evidently works as well in numerical calculations in those cases as it does for a free particle. However, to rigorously extend the discussion here to the Coulomb case would require an analysis of the complex coordinate behavior of Coulomb wave packets which we leave for a later investigation.

The application of these ideas to the Hamiltonians for charged particles in fields, which do not satisfy the condition that they be short range, turns out to be straightforward. In Sec. IV B we show that the contour $C(x)$ is applicable to a particle interacting with a dc field via the potential eE_0x. In Sec. IV C we show that the contour $D(x)$ in Fig. 2(b) is applicable to a particle in an ac field provided we work in the appropriate gauge. In both of these cases the complex contours we have discussed produce the same long time and large-x behavior as for the short-range case.

A final, but important, formal point concerns "time's arrow." We have discussed the limit $t\rightarrow\infty$, which is the one relevant to practical calculations where we begin with physically meaningful initial conditions at t_0 and propagate forward in time. If, on the other hand, we want to apply these ideas to the limit $t\rightarrow-\infty$, we must complex conjugate the contours $C(x)$ and $D(x)$. This fact is a reflection of the well-known association in formal scattering theory[33] of the $\pm\epsilon$ limits in the time-independent Green's function, e.g., in Eq. (11), with the $t\rightarrow\pm\infty$ limits in the propagator. If we were to modify Eqs. (11)–(13) to make the connection with the $-i\epsilon$ limit in the Green's function, the integral over time would be over the interval $[0,-\infty]$, and analytic continuation of the continuous spectrum of the Hamiltonian into the *upper* half plane would be necessary for convergence of the discrete representation in Eq. (7). The fact that changing the sign of θ (complex conjugating the contour) in a complex-coordinate calculation gives the $-i\epsilon$ limit has been discussed elsewhere.[34]

Another way to come to the same conclusion is to examine the free packet in Eqs. (14)–(18) in the $t\rightarrow-\infty$ limit, for which the behavior of α_t requires complex conjugation of the contour to produce the behavior described above for the $t\rightarrow\infty$ limit. In general, equivalent results are obtained by changing the direction of time evolution *and* the signs of *both* p_0 and θ.

III. COMPLEX FINITE-ELEMENT IMPLEMENTATION

All the numerical applications we discuss in the following sections were performed with a finite-element implementation of the construction of the propagator $\exp[-(i/\hbar)H(C(x))t]$ or $\exp[-(i/\hbar)H(D(x))t]$. A finite-difference procedure is in fact easier to implement using complex contours, but it is instructive to see how basis functions, even nonanalytic ones, can be used to represent the Hamiltonian on complex contours.

Our implementation follows Bottcher's[35] for real-valued coordinates, where the method can be viewed as an expansion of the wave packet $\Psi(x,t)$ in a basis of "tent functions" shown in Fig. 3 and defined by

$$\beta_n(x)=\begin{cases}(x-x_{n-1})/(x_n-x_{n-1}), & x_{n-1}<x<x_n\\ (x_{n+1}-x)/(x_{n+1}-x_n), & x_n<x<x_{n+1}\\ 0 \text{ otherwise.}\end{cases} \tag{21}$$

The points x_n form a grid, which may be unevenly spaced, and are called the "nodes" of the finite elements. The functions β_n lead to a tridiagonal representation of the Hamiltonian and a tridiagonal overlap matrix. Since only one function is nonzero at any node, and because its value is unity there, the coefficients in the expansion,

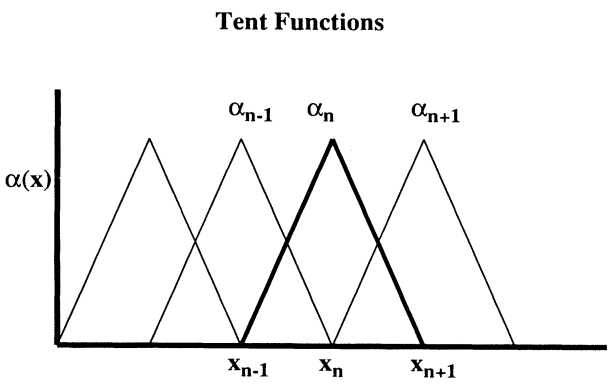

FIG. 3. Tent function basis for finite-element calculations.

$$\Psi(x,t)=\sum_{n=1}^{N} c_n(t)\beta_n(x) , \tag{22}$$

are the values of the wave function at the nth node. We have propagated the coefficients using the Cranck-Nicolson propagator,[36] which is a familiar unitary approximation in terms of the Hamiltonian and overlap matrices, $\underline{H}$ and $\underline{S}$,

$$\mathbf{c}(t+\Delta t)=\underline{U}(\Delta t)\mathbf{c}(t) , \tag{23}$$

with

$$\underline{U}\equiv\left[\underline{S}+\frac{1}{2\hbar}i\underline{H}\Delta t\right]^{-1}\left[\underline{S}+\frac{1}{2\hbar}i\underline{H}\Delta t\right]^{*} . \tag{24}$$

Extending this procedure for complex coordinates requires some simple modifications. If we use the exterior scaling contour $C(x)$, for example, we must deal with the fact that the conventional tent functions β_n are not continuous on that contour. So we define complex tent functions $\tilde{\beta}_n$ which are continuous on $C(x)$,

$$\tilde{\beta}_n(C(x))=\begin{cases}[C(x)-z_{n-1}]/(z_n-z_{n-1}), & x_{n-1}<x<x_n\\ [z_{n+1}-C(x)]/(z_{n+1}-z_n), & x_n<x<x_{n+1}\\ 0 \quad \text{otherwise,}\end{cases} \tag{25}$$

where we have moved the nodes onto the contour $C(x)$,

$$z_n=\begin{cases}x_n, & x_n<x_M\\ x_M+(x_n-x_M)e^{i\theta}, & x_n\geq x_M.\end{cases} \tag{26}$$

These complex finite elements $\tilde{\beta}_n(z)$ are continuous for z on the contour, $C(x)$, and share the property of the conventional "tent functions" that only one element is nonzero at any node, z_n, so that the coefficients in an expansion of the wave packet in terms of $\tilde{\beta}_n(z)$ are the values of the packet at the nodes. The next step is to construct the matrix elements according to a definition in terms of a contour integral,[2]

$$\underline{\tilde{H}}_{n,m}=\int_C \tilde{\beta}_n(z)H(z)\tilde{\beta}_m(z)dz . \tag{27}$$

This definition gives the correct analytic continuation of the finite-element method to complex values of the nodes. Simple formulas are thus obtained for the matrix elements of the kinetic energy and overlap. These matrix elements are given by the analytic continuation of the analogous expressions for real nodes to the complex values z_n of the nodes on the contour,

$$\tilde{T}_{n,n}=\frac{1}{2}\left[\frac{1}{z_n-z_{n-1}}+\frac{1}{z_{n+1}-z_n}\right] , \tag{28}$$

$$\tilde{T}_{n,n+1}=\tilde{T}_{n+1,n}=-\frac{1}{2}\left[\frac{1}{z_{n+1}-z_n}\right] , \tag{29}$$

$$\tilde{S}_{n,n}=\tfrac{1}{3}(z_{n+1}-z_{n-1}) , \tag{30}$$

$$\tilde{S}_{n,n+1}=\tilde{S}_{n+1,n}=\tfrac{1}{6}(z_{n+1}-z_n) . \tag{31}$$

The potential matrix elements are defined by the contour integral in Eq. (27) and were evaluated in all the calculations in this work with two-point Gauss quadrature on each interval $[z_n,z_{n+1}]$. The intervals may be complex, and the potential matrix is tridiagonal.

Since in complex-coordinate calculations the Hamiltonian and overlap matrices are complex symmetric instead of Hermitian the propagator in Eqs. (23) and (24) must be modified accordingly,

$$\underline{\tilde{U}}\equiv\left[\underline{\tilde{S}}+\frac{1}{2\hbar}i\underline{\tilde{H}}\Delta t\right]^{-1}\left[\underline{\tilde{S}}-\frac{1}{2\hbar}i\underline{\tilde{H}}\Delta t\right] . \tag{32}$$

Since the wave packet disappears as it propagates beyond x_M, its normalization changes after any part of it reaches that point. The propagator in Eq. (32) is correspondingly nonunitary, as it must be. The values of the coefficients in the expansion,

$$\Psi(z,t)=\sum_{n=1}^{N} \tilde{c}_n(t)\tilde{\beta}_n(z) , \tag{33}$$

give the values of the wave packets at the complex nodes,

$$\Psi(z_n,t)=\tilde{c}_n(t) , \tag{34}$$

to within the accuracy allowed by the choices of the numbers of finite elements and time steps.

IV. NUMERICAL EXAMPLES AND ANALYSIS FOR TIME-DEPENDENT POTENTIALS

In this section we provide numerical demonstrations of the ideas in Sec. II and extend them to the cases of charged particles in dc and ac electromagnetic fields. The numerical examples we discuss are all for electrons, and we use atomic units, in which $\hbar=1$, $m_e=1$, and $e=1$, when specifying the numerical parameters of the calculations.

A. Short-range potentials

In a previous publication[2] we presented an application to the potential $-1/x$ using the contour $C(x)$. To use the exterior scaling idea on the interval $-\infty<x<\infty$ we need to generalize the contour to $D(x)$, which is shown

in Fig. 2(b). To demonstrate that this approach works we have propagated a wave packet which bifurcates under the influence of the potential

$$V(x)=\exp\left[-\frac{x^2}{2}\right] . \tag{35}$$

The initial packet,

$$\Psi(x,0)=\exp\left[\frac{i}{\hbar}\alpha_0(x-x_0)^2+\frac{i}{\hbar}p_0(x-x_0)+\frac{i}{\hbar}\gamma_0\right] , \tag{36}$$

was chosen to be centered at $x_0=0$ with $p_0=0$, so that under the influence of the potential, pieces recede toward $x=\infty$ and $-\infty$. We chose $\alpha_0=0.5i$ and, here and in every example below, we chose γ_0 so as to normalize the wave packet. The parameters of the generalized exterior scaling contour, $D(x)$ were $\theta=20°$ and $x_M=15$.

The results of this propagation are given in Fig. 4, which shows the sudden decay of the packet outside of the interval $[x_M,-x_M]$. The propagation was carried out for time steps $\Delta t=0.01$ with 450 equally spaced finite elements on the interval $[-22.5,22.5]$. Ordinary propagation using real coordinates on this interval leads to dramatic spurious reflections from the grid boundaries as shown in the figure. Figure 4 also includes a packet propagated without complex coordinates and with 1200 finite elements on the larger interval $[-50,50]$. Agreement to 4 significant figures is obtained on the interval $[x_M,-x_M]$ between this calculation and the one using the complex contour.

In this calculation, as well as in the others we discuss, the accuracy of the calculation on the interval $[x_M,-x_M]$ can be increased without limit by choosing smaller spatial intervals and time steps, together with larger scaling angles. It is easy to show that the larger the scaling angle the sharper the decline of the packet past x_M, and therefore the smaller its value at the edge of the finite-element grid. However, increasing the scaling angle can also make the vicinity of the point x_M require more elements for an accurate treatment.

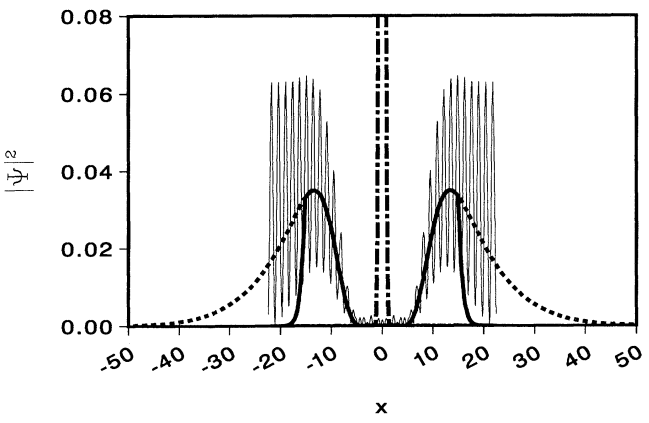

FIG. 4. Bifurcating packet for the Gaussian potential using the contour $D(x)$. Dash-dotted line denotes $t=0$, and heavy solid line denotes $t=10$. Light solid line shows reflections from the grid boundary for propagation on the same interval but without complex contour, while heavy dashed line is the same packet propagated to $t=0$ without complex contours but using a larger number of elements on an extended interval.

B. Particle in a dc field

For a particle of charge e in a uniform dc field the Hamiltonian is

$$H=\frac{p^2}{2m}+eE_0x , \tag{37}$$

which is familiar from discussions of the Stark effect in atoms.[37] It is a simple matter to follow the approach of Heller[32] to solve the TDSE in this case and show that a Gaussian wave packet,

$$\Psi(x,t)=\exp\left[\frac{i}{\hbar}\alpha_t(x-x_t)^2+\frac{i}{\hbar}p_t(x-x_t)+\frac{i}{\hbar}\gamma_t\right] , \tag{38}$$

for this problem remains Gaussian, and that it is an exact solution with time-dependent parameters given by

$$x_t=x_0+\frac{p_0}{m}(t-t_0)-\frac{eE_0}{2m}(t-t_0)^2 , \tag{39}$$

$$p_t=p_0-eE_0t , \tag{40}$$

$$\alpha_t=\frac{\alpha_0}{\left[\frac{2}{m}\right]\alpha_0(t-t_0)+1} , \tag{41}$$

$$\gamma_t=-\frac{i\hbar}{4}\ln\left|\frac{2\alpha_0}{\pi\hbar}\right|+\frac{i\hbar}{2}\ln\left[\frac{2\alpha_0(t-t_0)}{m}+1\right]+\left[\frac{p_0^2}{2m}-eE_0x_0\right](t-t_0)-\frac{eE_0p_0}{m}(t-t_0)^2+\frac{(eE_0)^2}{3m}(t-t_0)^3 . \tag{42}$$

This packet spreads in exactly the same way that a free packet does, since α_t is the same, but its motion and phase are of course quite different. For our purposes, however, the essential feature of the packet is expressed in Eq. (40). Since the sign of p_t remains fixed and opposite to that of E_0 for large t, the arguments in the preceding section regarding the factor in Eq. (20) apply, as long as we choose the correct sign for the scaling angle, θ. For positive p_t, θ must be positive in the contour $C(x)$, while for negative p_t the contour must be chosen for negative x in the same way that $D(x)$ appears in Fig. 2(b). In fact, $D(x)$ produces the desired behavior for $t\rightarrow\infty$ for either sign of E_0.

C. Particle in an ac field

The Hamiltonian for a particle of charge e in an electromagnetic field is[37]

$$H=\frac{1}{2m}\left[\mathbf{p}-\frac{e}{c}\mathbf{A}\right]^2+e\phi\ , \tag{43}$$

where $\mathbf{p}$ is the momentum operator, and $\mathbf{A}$ and ϕ are the vector and scalar potentials. If we choose a gauge in which ϕ and the divergence of $\mathbf{A}$ are zero, the Hamiltonian becomes

$$H=\frac{\mathbf{p}^2}{2m}-\frac{e}{mc}\mathbf{A}\cdot\mathbf{p}+\frac{e^2}{2mc^2}A^2\ . \tag{44}$$

This form is known as the radiation gauge,[38,39] and it is in this gauge that complex contours are applicable in the time-dependent Schrödinger equation. Although it would be difficult to establish that this is the case for an arbitrary vector potential $\mathbf{A}$, we can demonstrate the result easily for a linearly polarized field described by a vector potential of the form

$$\mathbf{A}=a\hat{\epsilon}\cos(\omega t) \tag{45}$$

where $\hat{\epsilon}$ is a unit vector in the x direction. The Gaussian wave-packet solution of the time-dependent Schrödinger equation for this problem is a special case of the Volkov packet.[38–40] The y and z motion is the same as for the free packet, and we must solve the TDSE for the x motion,

$$i\hbar\frac{\partial}{\partial t}\Psi(x,t)=\left[\frac{p_x^2}{2m}-\frac{ea}{mc}\cos(\omega t)p_x+\frac{e^2a^2}{2mc^2}\cos(\omega t)^2\right]\Psi(x,t)\ . \tag{46}$$

Again, if we write the solution in the form of Eq. (38) it is straightforward to show that the evolution of the packet is given exactly by

$$x_t=x_0+\frac{p_0}{m}t-\frac{ea}{\omega mc}\sin\omega t\ , \tag{47}$$

$$p_t=p_0\ , \tag{48}$$

$$\alpha_t=\frac{\alpha_0}{\frac{2\alpha_0 t}{m}+1}\ , \tag{49}$$

$$\gamma_t=-\frac{i\hbar}{4}\ln\left|\frac{2\alpha_0}{\pi\hbar}\right|+\frac{i\hbar}{2}\ln\left[\frac{2\alpha_0 t}{m}+1\right]+\frac{p_0^2}{2m}t-\frac{a^2e^2}{4mc^2}t-\frac{a^2e^2}{4mc^2\omega}\sin\omega t\cos\omega t\ , \tag{50}$$

where we have chosen $t_0=0$ for simplicity.

Note that α_t is the same as that of the free Gaussian packet. The critical feature of Eqs. (47)–(50) for our purposes is that p_t has fixed sign even though the center of the packet, x_t, contains a term which is oscillatory. For that reason, the discussion in Sec. II of the factor $\exp\{(i/\hbar)p_t[C(x)-x_t]\}$ in Eq. (20) still applies in this case. Furthermore, we can accommodate either sign of p_t by using the contour $D(x)$.

In Fig. 5 we show the propagation, using the contour $D(x)$, of the Gaussian packet describing the motion in this gauge of an electron in a field with $a/c=2$ and $\omega=0.5$ (atomic units). The same procedure works in the case that we add a short-range potential to the Hamiltonian, and as we show below, is applicable to the treatment of an atom in the ac field.

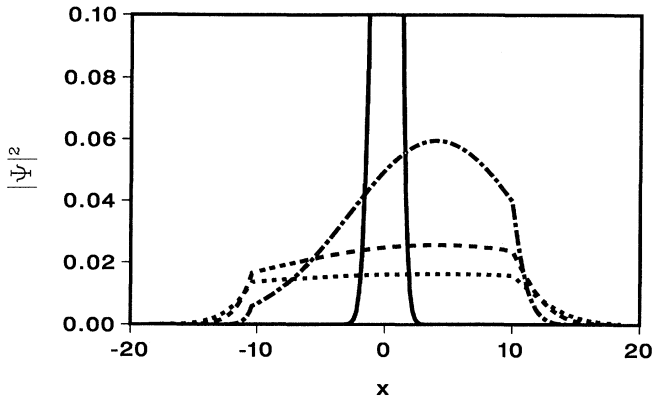

FIG. 5. Wave packet for a particle in an ac field. Solid line denotes $t=0$, dashed-dotted line denotes $t=3\pi$, dashed line denotes $t=7\pi$ and dotted line denotes $t=11\pi$.

We can accomplish the gauge transformation which brings the TDSE from the radiation gauge into the electric field gauge by applying the unitary transformation[38]

$$M=\exp\left[-i\frac{ae}{\hbar c}x\cos\omega t\right] \tag{51}$$

to Eq. (46). Defining the wave function in the electric field gauge, $\tilde{\Psi}(x,t)$, by

$$\tilde{\Psi}(x,t)=M\Psi(x,t)\ , \tag{52}$$

we obtain the familiar form

$$i\hbar\frac{\partial}{\partial t}\tilde{\Psi}(x,t)=\left[\frac{p_x^2}{2m}-eE_0x\cos\omega t\right]\tilde{\Psi}(x,t)\ , \tag{53}$$

where

$$E_0=\frac{a\omega}{c}\ . \tag{54}$$

It is useful to cast $\tilde{\Psi}(x,t)$ into the form of Eq. (38) in order to see how it behaves on complex contours. If we do so, setting t_0 to zero, the time dependence of the parameters is

$$x_t=x_0+\left[p_0+\frac{ea}{c}\right]\frac{t}{m}-\frac{ea}{\omega mc}\sin(\omega t)\ , \tag{55}$$

$$p_t=p_0-\frac{ea}{c}[\cos(\omega t)-1]\ , \tag{56}$$

$$\alpha_t=\frac{\alpha_0}{\frac{2\alpha_0 t}{m}+1}\ , \tag{57}$$

$$\gamma_t = -\frac{i\hbar}{4}\ln\left|\frac{2\alpha_0}{\pi\hbar}\right| + \frac{i\hbar}{2}\ln\left[\frac{2\alpha_0 t}{m}+1\right] + \frac{\left[p_0+\frac{ea}{c}\right]^2}{2m}t - \frac{a^2e^2}{4mc^2}t + \frac{3a^2e^2}{4mc^2\omega}\sin\omega t\cos\omega t - \frac{ea}{mc}\left[p_0+\frac{ea}{c}\right]t\cos\omega t - \frac{ea}{c}x_0\cos\omega t \ . \quad (58)$$

To specify the packet in the electric field gauge which corresponds via Eq. (52) to the one we found in the radiation gauge, ea/c must be subtracted from p_0 for the radiation gauge to get p_0 for the electric field gauge packet. The position x_t oscillates in this gauge as it does in the radiation gauge, but the important feature of Eqs. (55)–(58) is that p_t is now oscillatory and may continue to change sign as time increases (depending on the field strength and p_0). Thus in the electric field gauge our arguments concerning the momentum-dependent factor of the wave packet on the complex contour will fail if p_t continues to change sign as time increases. For that reason, it is not fruitful to apply complex exterior scaling in this gauge, even though it is arguably the more physical one in which to visualize the physics of the situation.[40]

D. Model atom in an intense ac field

To demonstrate the utility and accuracy of this approach in practical calculations on multiphoton ionization we investigated a model used recently by Su, Eberly, and Javanainen[41] to study the possibility of electron localization in intense high-frequency radiation fields. In their model the bare atom is characterized by the long-range, asymptotically Coulombic binding potential

$$V(x) = -\frac{1}{(1+x^2)^{1/2}} \ . \quad (59)$$

We chose an example from Su, Eberly, and Javanainen with an electric field with frequency $\omega=0.52$ and strength $E_0=0.5$. The field is turned on smoothly over 5 optical cycles, and our calculation differs slightly from that of Su, Eberly, and Javanainen in that we turn on the vector potential in the radiation gauge using the prescription they apparently use for turning on the field in the electric field gauge. In Fig. 6 we compare the result of propagating the ground state of this potential for 200 atu (where 1 atu $=2.42\times10^{-17}$ s) using the contour $D(x)$ with $x_M=\pm25$ and 2000 finite elements on the interval $[-100,100]$ with propagation using real coordinates and 8000 finite elements on the interval $[-400,400]$. Both of these intervals and densities of finite elements are larger than they need to be, but the results nevertheless indicate the accuracy and efficiency of the complex contour calculation. We were able to reproduce the ionization rates of Su, Eberly, and Javanainen[41] for this and other field strengths using complex exterior scaling and much reduced coordinate space intervals.

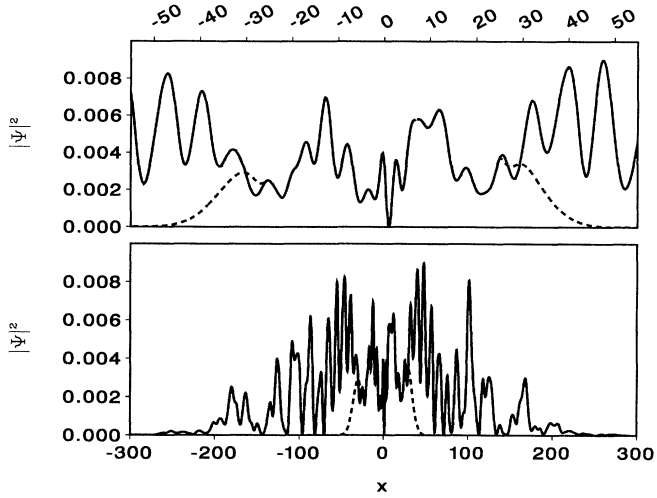

FIG. 6. Ionizing wave packet for one-dimensional hydrogen atom in an intense field; solid line is result from real coordinate propagation, and dashed line is from complex contour propagation. Upper panel shows magnification of vicinity of the atom.

E. Complex contours in more than one dimension for a scattering problem

To demonstrate the application of exterior scaling in more than one dimension, we have propagated a packet for an electron-hydrogen atom collision in an approximation[42] known as the "radial limit." In this picture the electron repulsion potential $1/|\mathbf{r}_1-\mathbf{r}_2|$ is replaced by its spherical average $1/r_>$. The two-electron Hamiltonian becomes (in a.u.)

$$H = -\frac{1}{2}\frac{\partial^2}{\partial r_1^2} - \frac{1}{2}\frac{\partial^2}{\partial r_2^2} - \frac{1}{r_1} - \frac{1}{r_2} + \frac{1}{r_>} \ , \quad (60)$$

where r_1 and r_2 are the distances from the nucleus to each of the two electrons. This problem is similar to that considered by Bottcher[35] in several studies of electron impact ionization of hydrogen, the difference being that in that work the electron repulsion potential was replaced by $1/(r_1+r_2)$. We have propagated an initial packet which corresponds to a high-energy electron incident on hydrogen in its ground state,

$$\Psi(r_1,r_2,0) = \frac{1}{\sqrt{2}}[\varphi(r_1,r_2)+\varphi(r_2,r_1)] \ , \quad (61)$$

where

$$\varphi(r_1,r_2) = 2r_2\exp(-r_2)(\pi^{1/2}d)^{-1/2} \times \exp\left[-ikr_1 - \frac{(r_1-a)^2}{2d^2}\right] . \quad (62)$$

This wave function is symmetric with respect to spatial coordinates and thus corresponds to singlet spin coupling of the incident and target electrons.

Since the coordinates are both on the interval $[0,\infty]$, we use the contour $C(x)$ for both r_1 and r_2. Figure 7

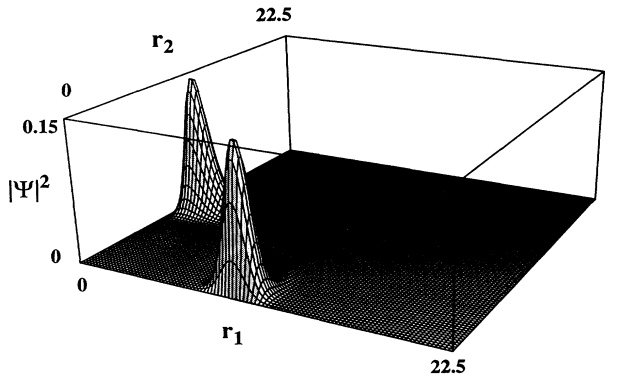

(a)

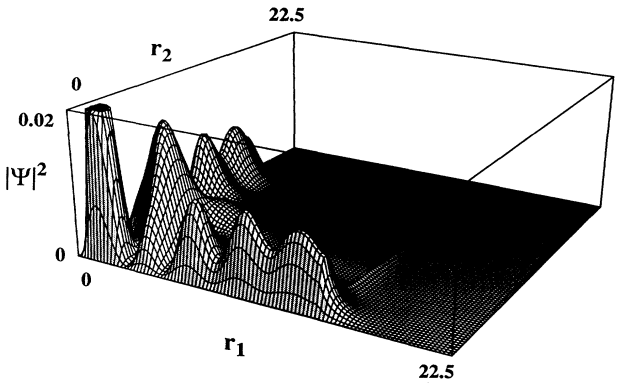

(b)

FIG. 7. Wave packet for electron-hydrogen collision in the radial limit: (a) $t=0$, (b) $t=10$.

shows the results of propagating the packet with $d=1$, $a=10$, and $k=2$ for 10 atu. The exterior scaling contours were chosen with $x_M=15$ and $\theta=20°$, and 100 evenly spaced finite elements were used on the total interval $0<r<22.5$. The decay of the final packet along the complex contours in both coordinates is apparent.

V. CONCLUSION

We have shown how to extend the method of complex coordinates to the time-dependent Schrödinger equation for a variety of cases. An elegant picture emerges from this effort which shows how the success of the complex-coordinate method in time-independent applications is connected to elimination of spurious periodic motion in the time-dependent representation as well as how the complex rotation angle is connected to "time's arrow." While we have not discussed the behavior of resonances in this picture, the techniques presented here provide a way to explore nonexponential decay of resonance states by separating the contribution due to the complex resonance pole from the remaining contributions. At a minimum, this idea provides a practical way to prevent spurious reflection of wave packets from grid boundaries, but there may be more utility beyond extinguishing outgoing packets.

To begin with, it is apparent that it is possible to analytically continue the packet back to the real axis numerically from the complex part of the exterior scaling contour. While this procedure might provide a way to recover the wave packet for some distance beyond the effective edge of the grid, it remains to be seen how stable the numerical analytic continuation will be. It is also possible to represent flux operator expressions for scattering amplitudes[34] on complex contours, so different ways of recovering scattering information from these packets may be possible.

We have also left some formal questions unanswered. We have not established the entire class of Hamiltonians for which complex exterior scaling is applicable in the TDSE to extinguish outgoing wave packets. In fact, we have only hinted what that class may contain and have not even given a proof for the Coulomb potential—for which the procedure evidently works perfectly. In addition, the application to a charge particle in an ac field raises the question of how these ideas might be applied in relativistic formulations of the problem.[38,39] We are exploring these questions as well as the relation of complex coordinates to complex time in the time-dependent Schrödinger equation.

ACKNOWLEDGMENTS

The authors wish to thank Ken Kulander and Lee Collins for enlightening conversations about the propagation of wave packets for atoms in fields. This work was supported by National Science Foundation Grant No CHE-8922836 and by a grant of computer time from the Ohio Supercomputer Center.

[1]S. D. Parker and C. W. McCurdy, Chem. Phys. Lett. **156**, 483 (1989).
[2]C. W. McCurdy and C. K. Stroud, Comput. Phys. Commun. (to be published).
[3]S.-I. Chu and W. P. Reinhardt, Phys. Rev. Lett. **39**, 1195 (1977); S.-I. Chu, Chem. Phys. Lett. **64**, 178 (1979).
[4]J. Aguilar and J. Combes, Commun. Math. Phys. **22**, 269 (1971); E. Balslev and J. Combes, *ibid.* **22**, 280 (1971); B. Simon *ibid.* **27**, 1 (1972).
[5]G. Doolen, J. Nuttall, and R. Stagat, Phys. Rev. A **10**, 1612 (1974); G. D. Doolen, J. Phys. B **8**, 525 (1975).
[6]R. A. Bain, J. N. Bardsley, B. R. Junker, and C. V. Sukumar, J. Phys. B **7**, 2189 (1974); B. R. Junker, Phys. Rev. A **27**, 2785 (1983).
[7]Y. K. Ho, Phys. Rev. A **23**, 2137 (1981); **38**, 6424 (1988).
[8]K. T. Chung and B. F. Davis, Phys. Rev. A **26**, 3278 (1982); B. F. Davis and K. T. Chung, *ibid.* **31**, 3017 (1985).
[9]C. W. McCurdy, J. G. Lauderdale, and R. C. Mowrey, J.

Chem. Phys. **79**, 2200 (1983); J. F. McNutt and C. W. McCurdy, Phys. Rev. A **27**, 132 (1983).

[10]C. W. McCurdy and T. N. Rescigno, Phys. Rev. Lett. **41**, 1364 (1978); J. G. Lauderdale, C. W. McCurdy, and A. Hazi, J. Chem. Phys. **79**, 2200 (1983); S. Yabushita and C. W. McCurdy, *ibid.* **83**, 3547 (1985).

[11]N. Moiseyev and C. T. Corcoran, Phys. Rev. A **20**, 814 (1979).

[12]Y. K. Ho, Phys. Rev. A **39**, 2709 (1989).

[13]J. Nuttall and H. L. Cohen, Phys. Rev. **188**, 1542 (1969).

[14]T. N. Rescigno and B. V. McKoy, Phys. Rev. A **12**, 422 (1975); T. N. Rescigno, C. W. McCurdy, and B. V. McKoy, J. Chem. Phys. **64**, 477 (1976).

[15]B. R. Johnson and W. P. Reinhardt, Phys. Rev. A **28**, 1930 (1983); B. R. Johnson and W. P. Reinhardt, *ibid.* **29**, 2933 (1984).

[16]T. N. Rescigno and C. W. McCurdy, Phys. Rev. A **31**, 624 (1985).

[17]C-h. Yu, R. M. Pitzer, and C. W. McCurdy, Phys. Rev. A **32**, 2134 (1985).

[18]B. R. Johnson, W. P. Reinhardt, C. W. McCurdy, and T. N. Rescigno, Phys. Rev. A **32**, 1998 (1985).

[19]B. Simon, Int. J. Quantum Chem. **14**, 529 (1978).

[20]I. W. Herbst, Commun. Math. Phys. **64**, 279 (1979); **75**, 197 (1980).

[21]I. W. Herbst, and B. Simon, Phys. Rev. Lett. **41**, 67 (1978); I. W. Herbst and B. Simon, Commun. Math. Phys. **80**, 181 (1981).

[22]C. Cerjan, W. P. Reinhardt, and J. E. Avron, J. Phys. B **11**, L201 (1978).

[23]A. Grossman and A. Tip, J. Phys. A **13**, 3381 (1980).

[24]W. P. Reinhardt, Annu. Rev. Phys. Chem. **33**, 233 (1982); A brief speculation in this review anticipates the possibility that complex coordinates might be used in time propagation.

[25]C. W. McCurdy, in *Resonances in Electron-Molecule Scattering, van der Waals Complexes, and Reactive Chemical Dynamics,* edited by D. G. Truhlar (American Chemical Society, Washington, D.C., 1984), Vol. 263, p. 17.

[26]C. W. McCurdy, in *Autoionization,* edited by A. Temkin (Plenum, New York, 1985), p. 135.

[27]B. R. Junker, Adv. At. Mol. Phys. **18**, 207 (1982); B. R. Junker, in *Autoionization,* edited by A. Temkin (Plenum, New York, 1985), p. 103.

[28]Y. K. Ho, Phys. Rep. **99**, 1 (1983).

[29]B. Simon, Phys. Lett. **71A**, 211 (1979).

[30]D. Neuhasuer and M. Baer, J. Chem. Phys. **90**, 4351 (1989); **91**, 4651 (1989).

[31]J. Turner and C. W. McCurdy, Chem. Phys. **71**, 127 (1982); R. Lefebvre, in *Resonances in Electron-Molecule Scattering, van der Waals Complexes, and Reactive Chemical Dynamics,* edited by D. G. Truhlar (American Chemical Society, Washington, D.C., 1984), Vol. 263, p. 35.

[32]E. J. Heller, J. Chem. Phys. **62**, 1544 (1975), describes a procedure for generating equations of motion for the parameters of Gaussian wave packets which can be extended to any Hamiltonian which is a quadratic form of momentum and position.

[33]R. G. Newton, *Scattering Theory of Waves and Particles* (Springer-Verlag, New York, 1982), p. 176.

[34]C. W. McCurdy and T. N. Rescigno, Phys. Rev. A **35**, 657 (1987).

[35]C. Bottcher, J. Phys. B **14**, L349 (1981); C. Bottcher, Adv. At. Mol. Phys. **20**, 241 (1985).

[36]R. Varga, *Matrix Iterative Analysis* (Prentice-Hall, Englewood Cliffs, NJ, 1962).

[37]L. I. Schiff, *Quantum Mechanics* (McGraw-Hill, New York, 1968), pp. 252 and 398.

[38]H. R. Reiss, Phys. Rev. A **19**, 1140 (1979).

[39]H. R. Reiss, Phys. Rev. A **22**, 1786 (1980).

[40]L. A. Collins and A. L. Merts, Phys. Rev. A **37**, 2415 (1988).

[41]Q. Su, J. H. Eberly, and J. Javanainen, Phys. Rev. Lett. **64**, 862 (1990).

[42]See, for example, C. W. McCurdy and T. N. Rescigno, Phys. Rev. A **40**, 1297 (1989).